Chapter 15
Silica and Alumina Nanophases: Natural Processes and Industrial Applications

Dominique J. Tobler, Tomasz M. Stawski, and Liane G. Benning

15.1 Introduction

Silicon (Si), aluminium (Al) and oxygen (O) are the three most abundant elements in the Earth's crust. The oxides these elements form constitute the main building block for silicate minerals, and they are most often the end member oxides in rock weathering processes. Due to their ubiquity, the variety of polymorphs they form, each unique in structure, property and reactivity, they are among the most useful natural materials.

Silica, usually denoted as SiO_2, can crystallise in many different crystal systems, forming a variety of polymorphs with stabilities governed by variable pressure and temperature conditions (Heaney et al. 1994). Among these, quartz is the most common and most stable form of SiO_2. When dissolved, the amount of silica in natural water is controlled by physicochemical parameters that are linked to

D.J. Tobler (✉)
Nano-Science Center, Department of Chemistry, University of Copenhagen, Copenhagen, Denmark
e-mail: dominique.tobler@nano.ku.dk

T.M. Stawski
German Research Centre for Geosciences, GFZ, D-14473 Potsdam, Germany

School of Earth and Environment, University of Leeds, LS2 9JT Leeds, UK

L.G. Benning
German Research Center for Geosciences, GFZ, Interface Geochemistry Section, 14473 Potsdam, Germany

Department of Earth Sciences, Free University of Berlin, 12249 Berlin, Germany

School of Earth and Environment, University of Leeds, Leeds LS2 9JT, UK

A.E.S. Van Driessche et al. (eds.), *New Perspectives on Mineral Nucleation and Growth*,
DOI 10.1007/978-3-319-45669-0_15

water–rock interactions (e.g. weathering) or biomineral growth (e.g. diatoms or radiolarians). These can vary significantly between different natural environments, e.g. 100 ppb in seawater to >1000 ppm in near-boiling pressurised geothermal waters. At Earth surface conditions, when SiO_2 levels become supersaturated, silica precipitates as an amorphous phase. Such amorphous silica, often referred to as opal-A, has a local structural coherence smaller than 20 Å, and its solubility, density, hardness and composition (e.g. water content can vary between 1 and 15 %) are highly dependent on precipitation conditions (Perry and Keeling-Tucker 2000). Yet, over time opal-A is unstable and gradually transforms into more crystalline phases and eventually to quartz. The time scale for this transformation process is highly dependent on the physicochemical conditions (i.e. temperature, pressure, pH conditions) (Williams and Crerar 1985) and can take tens of thousands of years (Herdianita et al. 2000).

The alumina system (Al_2O_3–H_2O) is notoriously more complicated, with different polymorphs forming under different temperature and pressure conditions but also at different solution pH. Aqueous Al^{3+} oxy-species (i.e. the aluminates) form as products of aqueous dissolution of aluminosilicates (which make up ~75 % of the Earth's crust) or of simpler $Al(OH)_3$, AlOOH and Al_2O_3 phases, with the highest dissolution rates occurring at acidic and alkaline conditions. In solutions supersaturated with regard to aluminate, typically only $Al(OH)_3$ and AlOOH phases precipitate, whereas Al_2O_3 or complex aluminosilicate phases are kinetically inhibited and usually only form at higher temperatures. In the pure alumina system, about half a dozen of metastable oxide and oxyhydroxide polymorphs are known to exist, and these only transform at >1000 °C to the thermodynamically stable trigonal corundum (α-Al_2O_3). For a full review, see Levin and Brandon 1998 and references therein.

In both the Si and Al systems, the formation of amorphous and (micro)crystalline phases is preceded by hydrolysis and condensation reactions leading to various mono-, di- or polynuclear species (Iler 1979; Brinker and Scherer 1990). In the silica system, solution speciation (Fig. 15.1a) and the type and abundance of polynuclear silica species do not affect polymorph selection, although they are believed to influence the formation kinetics (Iler 1979; Rothbaum and Rohde 1979; Belton et al. 2012). In contrast, the versatility of hydrolysed alumina species (Fig. 15.1b) and the polynuclear complexes it forms, most likely affects alumina polymorph selection (Wefers and Misra 1987; Casey 2006; Sipos 2009). In this chapter, we review the current knowledge on the mechanisms and kinetics of polymerisation and precipitation for these two systems. For simplicity, they will be discussed separately, first focusing on the silica system, considering both processes in natural waters and industrial applications. For the alumina system, we will take into account the amphoteric character of the solid phases, and the precipitation process will be discussed separately for acidic and alkaline solutions.

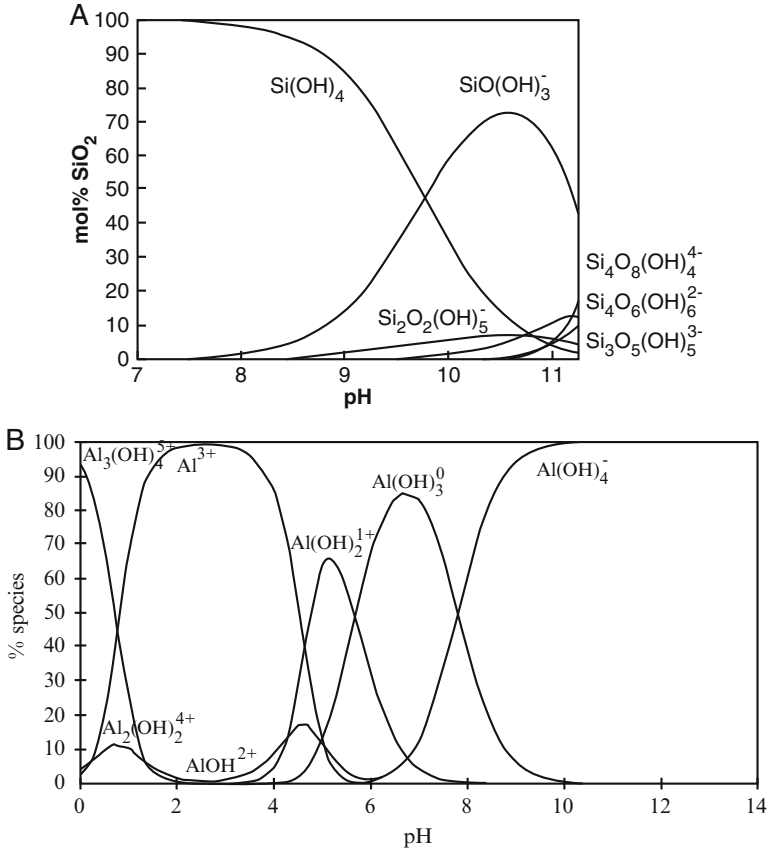

Fig. 15.1 Partial speciation diagrams of dissolved silica (**a**) and alumina (**b**) as a function of pH at 25 °C and 1 atm (Printed with permission from Elsevier from Dietzel (2000) for silica and Panias et al. (2001) for alumina)

15.2 Silica in Natural Waters

Silica polymerisation and the subsequent precipitation of silica occur in many modern terrestrial environments (e.g. hot springs, brines, marine sediments, rivers), and these processes are critical to a variety of processes including sinter formation, silica diagenesis and biosilicification (e.g. diatoms, sponges and plants) (Pancost et al. 2005; Perry and Keeling-Tucker 2000; Tobler et al. 2008), as well as the transport and fate of nutrients and contaminants, with silica nanoparticles acting as adsorbents or mobile carriers (Ryan and Elimelech 1996). Silica also played an important role in ancient geological settings; for example, most Archean fossils were preserved in silica cherts (Westall and Walsh 2000). Furthermore, such processes were likely also crucial in the formation of silica-rich deposits on Mars (Squyres et al. 2008) or on other extraterrestrial bodies with the recent discovery of silica-rich nanoparticles ejected from Enceladus, Saturn's sixth largest moon, pointing towards subsurface

hydrothermal processes (Hsu et al. 2015). The formation of silica in natural waters can also be a nuisance to industrial facilities and equipment, for example, during geothermal power extractions or in water treatment systems, where silica scaling and fouling can greatly reduce performance (Gunnarsson and Arnorsson 2005).

15.2.1 Silica Chemistry

In most natural waters, the silicate ion is usually present as orthosilicic acid, $Si(OH)_4$, a weakly acidic molecule (pKa 9.8), with the Si atom tetrahedrally coordinated to four hydroxyl groups. Orthosilicic acid remains stable as long as its concentration is below the solubility of amorphous hydrated silica (~110–120 ppm at 25 °C; Gunnarsson and Arnorsson 2000). Silica solubility is affected by several parameters, including pH, SiO_2 concentration, temperature, pressure and the presence of other ions, small molecules and polymers (Alexander 1954; Iler 1979; Rothbaum and Rohde 1979; Marshall and Chen 1982; Perry and Keeling-Tucker 2000; Gunnarsson and Arnorsson 2005; Patwardhan 2011). At the near-neutral pH of many natural waters, silica solubility is at its minimum, while it rapidly increases at pH values above 9, with orthosilicic acid becoming increasingly ionised (Fig. 15.1a). In acidic waters (pH < 3), the silica solubility is only slightly increased and silica polymerisation rates are at their lowest. Despite some discrepancy between reported solubility data, SiO_2 solubility increases with increasing temperature and/or pressure, while it generally decreases with an increase in ionic strength (IS). Naturally, IS favours the dissociation of acids, which in turn may enhance SiO_2 solubility (Fig. 15.1a), but likely this will only affect the solubility at pH close to the pKa. The lack of such data hinders a more thorough discussion on IS effects. The effects of inorganic and organic additives on silica solubility and polymerisation are highly variable, and the extent and the pathways in which they affect silica formation are still poorly quantified, but good insights can be found in Iler (1979) and Patwardhan (2011).

In solutions supersaturated with respect to amorphous silica, orthosilicic acid undergoes condensation reactions via the coalescence of orthosilicic acid molecules and the concurrent release of water:

$$Si(OH)_4 + Si(OH)_4 \leftrightarrow (HO)_3Si\text{–}O\text{–}Si(OH)_3 + H_2O$$

Further oligomerisation leads to the formation of trimers, tetramers, cyclic species and other polynuclear entities, thereby maximising the number of Si–O–Si bonds. Under most experimental conditions, the orthosilicic acid remains the dominant dissolved silica species (Icopini et al. 2005), while the composition and abundance of oligomers are primarily governed by pH and SiO_2 concentration but also temperature, ionic strength and the presence of other cations (Belton et al. 2012). These polynuclear species undergo condensation and dissolution processes up to a point where a critical cluster size is reached, and cluster growth becomes more likely than

cluster dissolution. This is also termed the nucleation barrier. Once reached, it leads to the formation of three-dimensional, internally condensed and highly hydrated silica nuclei, a few nanometres in size (Iler 1979). These nuclei can grow through monomer addition and/or through particle aggregation/coalescence (discussed in Sect. 15.2.2) and interact with the biochemical environment in which silica will be deposited. Overall, silica precipitates forming in surface waters are mostly amorphous (i.e. opal-A) and not affected by oligomer type or abundance (contrary to the alumina system, see Sect. 15.4). However, in some studies, silica precipitation rate laws have been inferred as being a consequence of polymerisation of certain oligomers (e.g. a fourth-order reaction corresponding to tetramer condensation) (Rothbaum and Rohde 1979). This is further discussed in the next section where the current understanding of silica formation mechanisms and kinetics is presented.

15.2.2 Silica Formation

The mechanisms of silica polymerisation and silica nanoparticle formation in natural systems have been widely investigated in both laboratory (Alexander 1954; Iler 1979; Carroll et al. 1998, 2007; Tobler et al. 2009; Tobler and Benning 2013; Kley et al. 2014) and field settings (Carroll et al. 1998; Mountain et al. 2003; Tobler et al. 2008; Meier et al. 2014), as well as through computational approaches (Noguera et al. 2015). Silica polymerisation and silica nanoparticle formation are generally described by a three-stage process where (1) silica polymerisation and nucleation of silica nanospheres are followed by (2) particle growth via accretion of silica monomers/oligomers and/or by Ostwald ripening and (3) particle aggregation.

In most natural waters (i.e. pH > 3), silica nanoparticles carry a negative charge, which becomes more negative with an increase in solution pH and/or ionic strength (Kobayashi et al. 2005; Barisik et al. 2014). This is explained by the deprotonation of surface silane groups as pH increases and a decrease in surface H^+ concentration with increasing ionic strength. Barisik et al. further observed that for particles with diameters < 100 nm, the negative surface charge increases with a decrease in particle size (Barisik et al. 2014). The higher the negative charge of the silica nanoparticles, the more likely it is that they remain in suspension (because of the electrostatic repulsion) and can get transported with the water flow. However, in most natural waters, silica nanoparticles are not stable within the polymerising solution and they aggregate into dense 3D networks. This is mostly due to IS effects, i.e. the presence of charged species (e.g. coagulating cations such as $Fe^{2+/3+}$ or Al^{3+}) or of "sticky" organic molecules (e.g. polysaccharides) that reduce and even neutralise the negative surface charge (Iler 1979; Perry and Keeling-Tucker 2000; Benning et al. 2005).

Early studies estimated the size of the first silica nanoparticles forming within the polymerising solution to be around 2–3 nm (Iler 1979). This was confirmed and visualised through atomic force microscopy analyses (Conrad et al. 2007). More recently, advances in scattering methods have made it possible to follow

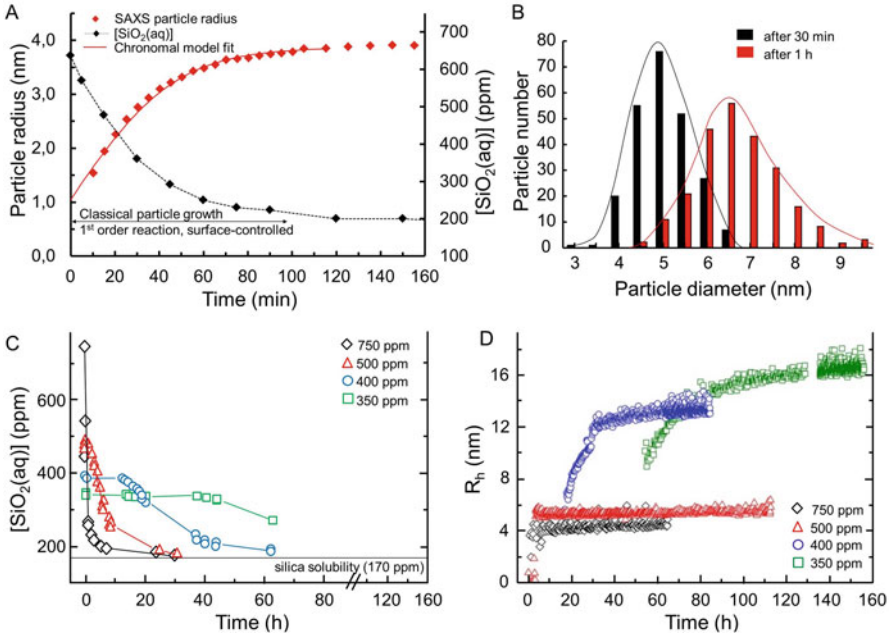

Fig. 15.2 (**a**) Initial steps of silica nanoparticle formation from supersaturated silica solutions monitored by SAXS (640 ppm SiO_2, IS = 0.22, pH = 7). Homogeneous nucleation followed by initial fast particle growth concomitant with the decrease in molybdate-reactive silica, [SiO_2(aq)] (modified after (Tobler et al. 2009). (**b**) Silica nanoparticle size distribution in polymerising solutions for two different ageing times (1600 ppm SiO_2, IS = 0.22, modified after Tobler et al. (2009)). (**c**) Decrease in monomeric silica and (**d**) concomitant growth of silica nanoparticles in solutions with varying initial silica concentrations as indicated (pH = 7; modified after Kley et al. (2014))

in situ and in a time-resolved manner the formation of silica nanoparticles from a polymerising solution. In Tobler et al. (2009), we combined synchrotron radiation small-angle X-ray scattering (SAXS) (Stawski and Benning 2013) and dynamic light scattering (DLS) flow-through experiments with (cryo)electron microscopy and monitored in situ the formation of silica nanoparticles from polymerising solutions where supersaturation was induced by a pH drop from about 12 to 7. These particles grew from 3 nm to approximately 8 nm, which was mirrored by a fast decrease in the orthosilicic acid concentration in solution (Fig. 15.2a, b). The size of the silica nanoparticles after 3h of polymerisation was not greatly affected by the tested silica concentrations (640 and 1600 ppm SiO_2) and ionic strengths (IS = 0.02–0.22), while particle aggregation initiated considerably earlier at higher SiO_2 concentrations and IS. Kley et al. (2014) followed a similar approach, employing both static and dynamic light scattering to monitor silica nanoparticle formation in pH-induced silica polymerising solutions at a wider range of SiO_2 concentrations (350–3000 ppm) and at two pH regimes (7 and 8). They showed that

the particle density increased and the final particle size decreased with increasing silica content (Fig. 15.2c, d) and pH, as expected from classical nucleation and growth theory. Similar to the work reported in Tobler et al. (2009), Kley et al. found that particle aggregation quickly set in at high SiO_2 concentrations and that at pH 7 aggregation was more enhanced than at pH 8 (Kley et al. 2014). They explained this as a consequence of an increase in negative surface charge on silica particles with increasing pH and with decreasing size and suggested that this leads to repulsive forces, inhibiting particle aggregation (Barisik et al. 2014; Kley et al. 2014). In an attempt to better mimic natural processes, where silica polymerisation and silica nanoparticle formation are the result of cooling (often extremely fast) of a high-temperature, silica-supersaturated near-neutral fluid to ambient (geothermal) or low temperatures (deep sea), we employed an approach similar to that used in Tobler et al. (2009) but used a high-temperature flow-through experimental system to monitor silica nanoparticle formation in temperature-induced silica polymerising solutions (Tobler and Benning 2013). Our results revealed that the rate at which silica nanoparticles formed was substantially lower (around 50 %) when polymerisation was induced by fast cooling as opposed to pH change (both systems having identical initial solution composition, i.e. [SiO_2]). This was evidenced by the occurrence of a lag time in the onset of particle growth, the formation of larger critical nuclei and the absence of particle aggregation in the temperature-induced experiments. This retardation in silica formation is explained by the differences in time to establish supersaturation: the radical change in pH (<30 s) imposed a faster attainment of supersaturated conditions compared to the slower (2–3 min) and more gradual change in T.

Although there are some differences in measured particle sizes and particle growth profiles between these three in situ studies (Fig. 15.2), they do however agree in the mechanistic interpretation of silica nanoparticle formation with silica polymerisation leading to the formation of condensed critical nuclei, which grow by addition of monomers according to classical growth theory up to the point where silica solubility is reached and/or particle aggregation sets in (Fig. 15.2a). Ostwald ripening has been suggested to be an important growth mechanism during the late stages of silica particle growth (Iler 1979; Perry and Keeling-Tucker 2000); however this process could not be identified at the conditions tested in these studies. Ostwald ripening seems particularly unlikely at higher SiO_2 concentrations (>1000 ppm SiO_2), where particle aggregation quickly follows particle growth.

Several studies have observed the occurrence of a lag time (i.e. induction period), where no silica polymerisation and particles are detected (i.e. no significant X-ray/light scattering above background), although at the start of these experiments, the experimental solutions were already at maximum supersaturation (Rothbaum and Rohde 1979; Tobler and Benning 2013; Kley et al. 2014). The length of this induction period is controlled by the same factors that determine silica solubility (i.e. T, pH, IS and [SiO_2]), and it decreases with an increase in silica supersaturation (Iler 1979; Rothbaum and Rohde 1979; Gunnarsson and Arnorsson 2005; Conrad et al. 2007). It is generally accepted that induction periods, recently also described

as supersaturation plateaus (Noguera et al. 2015), represent the time during which larger polymeric cluster structures and/or particles form and dissolve again (Perry and Keeling-Tucker 2000), in agreement with classical nucleation theory. Such large structures could be similar to the pre-nucleation clusters suggested for other mineral systems (e.g. $CaCO_3$; De Yoreo et al. 2017, Chap. 1). In both the silica and calcium carbonate systems, particle nucleation likely occurs once such cluster structures become dense enough to form the first solid particle.

This shows that despite the extensive research carried out in this field, there are still a few gaps in the molecular-level mechanistic understanding of the nucleation and growth of primary silica particles in natural aqueous solution. This is further illustrated by the variety of kinetic models that have been derived from measurements of the time-dependent decrease in orthosilicic acid concentration or silica nanoparticle growth profiles, with reaction orders ranging between 1 and 6 (Tobler et al. 2009; Tobler and Benning 2013; Kley et al. 2014; Noguera et al. 2015) and with varying dependencies on, for example, pH, $[SiO_2]$, particle surface area or oligomer type. Due to the massive interest of industry in the production of monodisperse silica nanoparticle, the bulk of the research has focused on the mechanistic and kinetic understanding of silica nanoparticles synthesised using organosilanes as a precursor (see Sect. 15.2.3). However, differences in the formation process may prevent the resulting models from being applied to inorganic natural systems.

15.2.3 Silica for Industrial Applications

Silica nanoparticles are highly desirable materials for industrial applications (e.g. electronics, biotechnology, catalysis, water purification and chromatography) because of their specific structural properties (e.g. swelling capacity, strength, durability, thermal stability, dielectric properties) (Ab Rahman and Padavettan 2012; Hench and West 1990; Bagwe et al. 2006; Wang et al. 2008). In natural waters, silica is formed from an inorganic building block, i.e. orthosilicic acid, while most synthetic silica nanoparticles are produced through the hydrolysis and condensation of alkoxysilanes, for example, tetraethoxysilane (TEOS) and tetramethoxysilane (TMOS). Highly monodisperse, spherical silica particles have been obtained through the so-called Stöber method (the base catalysed hydrolysis and condensation of alkoxysilanes in low-molecular-weight alcohols) (Stöber et al. 1968), but other processes such as the diffusion of alkoxysilanes into a stirred aqueous solution of lysine have also been investigated (Yokoi et al. 2006). In aqueous solutions with acidic or basic catalysts, alkoxyl groups are hydrolysed to form silanol groups and alcohol. The condensation between silanol groups (Si–OH) or between silanol and alkoxides (Si–OR) group creates siloxane bridges (Si–O–Si). These processes are affected by the type of alkoxysilane, the nature and composition of solvent and catalyst, temperature, pH, as well as reactant mixing procedures (Ab Rahman and Padavettan 2012; Besselink et al. 2013), which can be tuned to

produce specific particle sizes and distributions. Silica nanoparticles prepared with alkoxysilanes have much smoother surfaces compared to silica particles formed by the condensation of orthosilicic acid in water. This is argued to be due to the reversible exchange of alkoxyl (Si–OR) and hydroxyl (Si–OH) groups, thereby creating a relaxation mechanism for further smoothening, while condensation of orthosilicic acid produces fixed Si−O−Si bonds (Carcouet et al. 2014).

The formation conditions for industrial silica nanoparticles greatly differ from those in nature, thus the reaction kinetics and mechanisms, to form highly size-controlled, smooth and monodispersed silica nanoparticles during the hydrolysis and condensation of alkoxysilanes, naturally deviate from those that occur in nature (Sect. 15.2.2). However, there are quite a few similarities discussed below. Scattering and spectroscopy techniques combined with (cryogenic) electron microscopy and molecular modelling have provided evidence that silica polymers with an open fractal structure are the early species, which, once sufficient levels of supersaturation are reached, transform into a dense sphere, with a size of approximately 2 nm (Boukari et al. 2000; Green et al. 2003; Fouilloux et al. 2011; Carcouet et al. 2014). However, there is still debate on the mechanistic steps that lead to the monodispersed mature particles formed during the hydrolysis and condensation of alkoxysilanes, possibly also because of the large number of parameters that impact these processes (i.e. type and concentration of alkoxysilane, solvent and catalyst, mixing procedure, etc.). Similar to silica nanoparticle formation in natural systems, growth by monomer addition (classical growth theory) has been a suggested mechanism (Matsoukas and Gulari 1989). Several studies have argued, however, that the observed particle growth trends could also be explained by particle aggregation (Bogush and Zukoski 1991). In the monomer addition model, nucleation occurs in the initial stages leading to the formation of a set number of nuclei, which then grow by the addition of hydrolysed monomers. On the other hand, in the aggregation model, nucleation occurs continuously throughout the reaction, producing nuclei of a certain size, which first aggregate to form larger particles and then grow by further addition of the primary nuclei. A recent study combining high-resolution cryogenic transmission electron microscopy (TEM) with ^{29}Si magic angle spinning (MAS) nuclear magnetic resonance (NMR) gives convincing evidence of the formation of monodisperse silica nanoparticles through the aggregation of uniform 2.3 nm sized primary particles to larger (>10 nm) units (Fig. 15.3) (Carcouet et al. 2014). These larger units grow by further addition of primary particles, which collapse upon association from 2.3 nm in solution to about 1.3 nm when bound to an aggregate (associated with the expulsion of water). They further showed that free primary particles were present at all stages of particle growth (Fig. 15.3), which demonstrates that nucleation occurs throughout the reaction. Further support for the aggregation model comes from a seeded growth experiment (Bogush and Zukoski 1991), where the decrease in orthosilicic acid concentration was unaffected by the number density of particles, which suggested that particle growth did not occur via direct condensation of monomers onto the particle surface. In the aggregation model, the fast initial decrease in orthosilicic acid concentration (i.e. fast consumption of monomers once the reaction is induced) is explained by the formation of ionised,

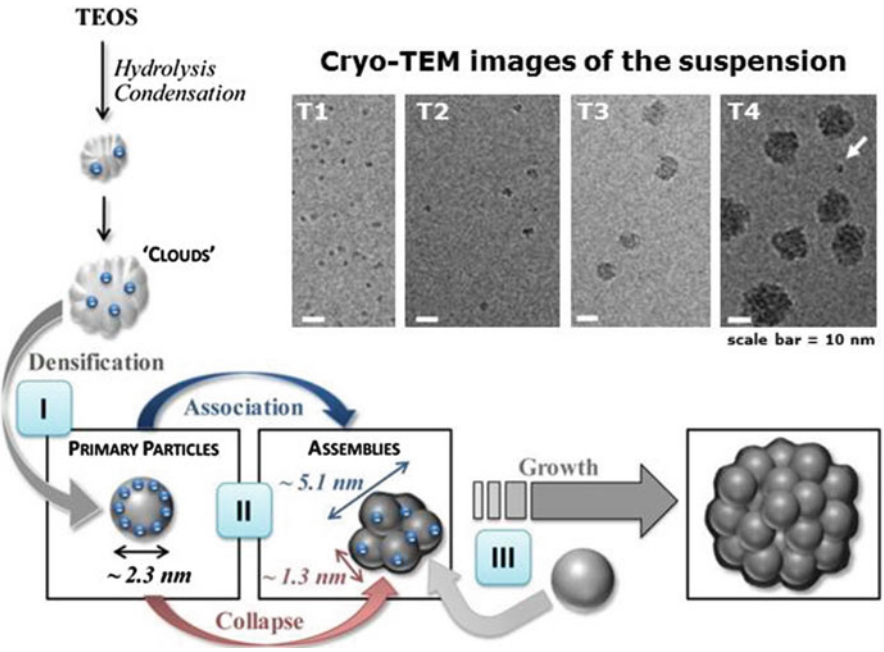

Fig. 15.3 Schematic representation of silica nanoparticle formation mechanism modified after Carcouet et al. (2014). Initial open structures densify to primary particles (Stage I; T1) that collapse upon association into assemblies (Stage II; T2, T3). After association, no further new assemblies are formed, and growth occurs via the addition of primary particles (Stage III; T4, arrows point at a free primary particle)

open structures of low density that collapse to form primary particles. This leads to a steady increase in particle density up to a point where these primary particles start to aggregate into more stable assemblies, leading to a sharp decrease in particle density. Following formation of these assemblies, the particle number remains stable, and the decrease in orthosilicic acid concentration proceeds at a much lower rate (producing new primary particles for growth through aggregation). Similarly, Fouilloux et al. reported an initial fast increase in the particle number density up to a plateau, where particle numbers remained constant, but particle growth still occurred (Fouilloux et al. 2011). They argued that this result supports a mechanism with two consecutive phases: (a) nucleation and growth and then followed by (b) phase densification. However, as pointed out by Carcouet et al., it could also be that primary particles with sizes lower than 3 nm were present but simply not visible by the employed techniques of these previous studies (Carcouet et al. 2014). Also, the usually observed plateau in particle number density occurring during the particle growth process can be easily explained with the aggregation processes described above.

15.3 Alumina in Natural Waters and in Aqueous Industrial Environments

Aluminium is contained in more than 250 different minerals, most noteworthy in the form of common aluminosilicates (e.g. feldspars or clays) and the economically important bauxite ore (mixed Al oxides and hydroxides). Rock weathering and soil formation processes are to a large extent driven by the interaction of fluids with rocks leading to the dissolution of these various phases containing Al. Similar to silica nanoparticles, colloids in the alumina–water system control the cycling of various species in natural waters by introducing a charged solid-liquid interface to which a multitude of inorganic (e.g. phosphate, arsenic, lead, iron, chromium) and organic (e.g. humic acid) compounds can adsorb (Kasprzyk-Hordern 2004). This way alumina colloids are involved in cycling of anthropogenic pollutants in soils and natural waters and have many applications in water treatment (Hu et al. 2006). Al-containing compounds and their processing are also essential for various industries, for example, metallurgy and welding, ceramic production, catalysis, electronics, pharmaceutics, cosmetics, fire prevention, paint production, etc. (Wefers and Misra 1987; Levin and Brandon 1998).

The main difference between the alumina–water and silica–water systems is that in the alumina system, there are a multitude of possible Al-oxyhydroxide phases that can precipitate from solution. Typically, amorphous colloids form at the beginning and then transform directly in solution to crystalline polymorphs (Wefers and Misra 1987). It is generally accepted for the alumina system that the reaction pathways and the products strongly depend on the Al speciation in solution. The various aqueous Al^{3+} oxy-species (i.e. the aluminates) form through dissolution of amphoteric Al phases under acidic and alkaline conditions, as illustrated in Fig. 15.1b. In natural waters, the precipitation of Al phases usually occurs through the neutralisation of Al-rich acidic solutions (pH > 3–4), while in industrial settings, the neutralisation is most often from alkaline liquors (pH < 9–10, i.e. the Bayer process used for processing of bauxite ores). Unsurprisingly, due to the geochemical and industrial importance of the alumina system, a substantial body of literature on precipitation from solution as well as speciation of aqueous entities exists (e.g. see the reviews by Wefers and Misra (1987), Swaddle et al. (1994), Casey (2006), Sipos (2009) and references therein). Below we present a brief summary of the current knowledge.

15.3.1 Solid Phases in the Alumina–Water System

The water–alumina system is characterised by a plethora of polymorphs, and thus it is inevitable to consider first the possible solid products of precipitation from the aluminate solutions. Excluding pure Al_2O_3 phases (since they typically do not

precipitate from solution), these include (Wefers and Misra 1987; Ruan et al. 2001; Kloprogge et al. 2006; Demichelis et al. 2009; Smith et al. 2013):

- Colloidal amorphous and gelatinous hydrated alumina(s) formed through condensation of aluminate complexes (Bale and Schmidt 1959; Petz 1968; Nail et al. 1976a, b, c; Rousseaux et al. 2002) and including all nanometre-sized amorphous oxides, hydroxides and oxyhydroxides.
- Poorly crystalline pseudo-spinel (Bradley and Hanna 1994) and pseudo-boehmite structures formed through ageing of the amorphous phases mentioned above and containing up to 30 wt% water with respect to the Al_2O_3 stoichiometry (Tettenhorst and Hofmann 1980; Wefers and Misra 1987; Brinker and Scherer 1990). Further ageing of pseudo-boehmite leads to either trihydroxide(s) (at $T < \sim 75$ °C) or oxyhydroxide(s) ($T > 75$°C) (Wefers and Misra 1987).
- Crystalline Al-trihydroxides ($Al(OH)_3$), in which the Al^{3+} is octahedrally coordinated by OH^- groups, and each OH^- is bound to two cations with a vacant third octahedron, thus forming neutral sheet structures (Demichelis et al. 2009). The most studied $Al(OH)_3$ phases are:
  - Gibbsite, the most common and thermodynamically stable phase among hydroxides in natural systems (major component in bauxite ore). Structurally it contains OH^- ions in consequent and opposite layers with a sequence arranged as {−AB-BA-AB-BA-...} in the direction perpendicular to the layers – it means that OH^- ions of the adjacent groups are located directly in front of each other (Fig. 15.4a) (Saalfeld and Wedde 1974).
  - Bayerite, which crystallises under highly basic conditions during processing of bauxites (i.e. the Bayer process). Its layers follow the sequence {−AB-AB-...} – OH^- ions from one layer are shifted in respect to the previous one, so that the ions from one layer fall into spaces in-between hydroxyls from the neighbouring ones (Fig. 15.4a) (Rothbauer et al. 1967).
  - Nordstrandite, which crystallises upon ageing of precipitates at mildly basic conditions (pH ∼ 7.5–9). Its structure follows the bayerite layer pattern, but with oppositely located hydroxyl groups, hence yielding the sequence {−AB-AB-BA-BA-...}(Fig. 15.4a) (Saalfeld and Jarchow 1968).
  - Doyleite, only discovered recently (Caho et al. 1985), has a similar layer stacking as bayerite (Fig. 15.4a), but the hydroxyls of the two consequent double layers are located in intermediate positions between those of gibbsite and nordstrandite (Demichelis et al. 2009).
- Al-oxyhydroxides (AlOOH) are composed of double layers, in which the primary motif 2 AlOOH forms chains (Wefers and Misra 1987):
  - Boehmite, precipitating upon neutralisation of aluminate solutions at elevated temperatures, in which 2 AlOOH-based chains are arranged in a cubic packing (Fig. 15.4a) (Christoph et al. 1979).
  - Diaspore, in which the 2 AlOOH-based chains are arranged in a hexagonal packing (Fig. 15.4a) (Busing and Levy 1958). This phase is typically found as the product of weathering or high-temperature transformations (Keller 1978).

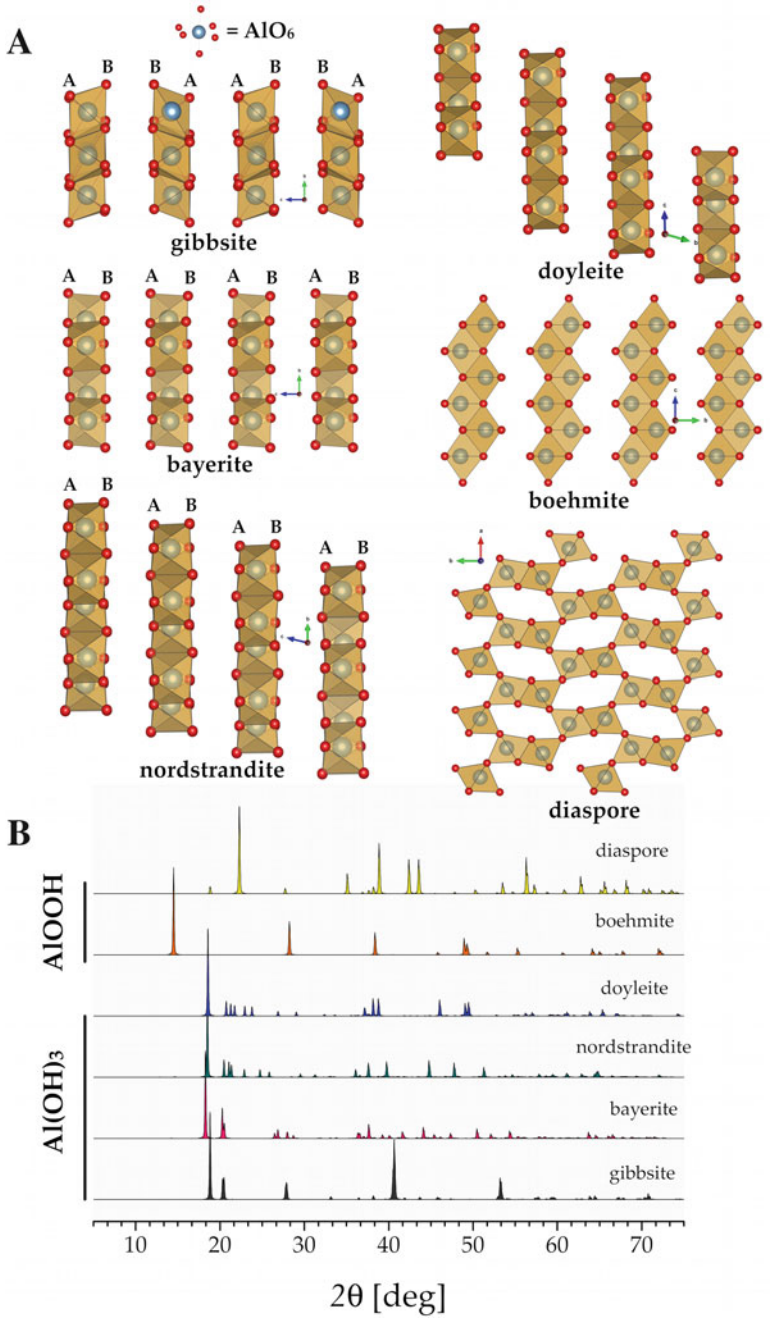

Fig. 15.4 (**a**) Structures of aluminium oxy-hydroxide phases in octahedral representations. (**b**) Simulated diffraction patterns of the same phases for the wavelength corresponding to Cu $K_{\alpha 1}$. Patterns and visualisations were generated from the structural information contained in the following entries of the ICSD: gibbsite, 98-000-6162; bayerite, 98-002-6830; nordstrandite, 98-003-4393; doyleite, 98-005-0581; boehmite, 98-003-6340; diaspore, 98-001-6768. Visualisations and diffraction pattern simulations were prepared in VESTA 3 (Momma and Izumi 2011)

These differences are translated into variations in the diffraction patterns of the various crystalline phases (Fig. 15.4b), which show common structural features among the trihydroxide group phases in more stark contrast to the oxyhydroxides.

The Al speciation diagram in Fig. 15.1b clearly shows the precipitation region for solid trihydroxides at pH ~4 to ~10. Precipitation has been shown to occur during the neutralisation of the acidic and alkaline aluminate solutions and proceeds through a colloidal stage with possible polynuclear complex ions and their condensation products, as will be explained in more detail in the sections below. In both cases, an initially formed amorphous alumina gel eventually transforms to pseudo-boehmite, which has fibrous and sheetlike morphologies. This pseudo-boehmite only gradually crystallises to bayerite and gibbsite (Cesteros et al. 1999) through the following sequence:

Colloidal amorphous or gelatinous alumina (s) → pseudo-spinel and pseudo-boehmite → bayerite → gibbsite

The polymorphic sequence as well as the morphology and the size distribution of the products depend strongly on the physicochemical conditions of the precipitation and transformation reactions (Li et al. 2005a, b, 2011). Gibbsite and bayerite can crystallise concurrently from aluminate solutions, yet this transformation depends on chemical conditions and bayerite is also known to transform to gibbsite (Loh et al. 2000; Li et al. 2005b, 2011). In strongly caustic environments and at temperatures close to 100 °C, boehmite can form instead of trihydroxides (gibbsite or bayerite) (Wefers and Misra 1987; Gong et al. 2003). The kinetics and mechanisms for these polymorphic transformations between the various Al phases are still not fully understood, partly because we lack knowledge of their stability field. Indeed, gibbsite is regarded as the most stable phase because it is most common, but clear evidence is missing. For more details, the reader is referred to the excellent reviews and summaries found in Wefers and Misra (1987), Loh et al. (2000), Gong et al. (2003), Li et al. (2005a) or Li et al. (2011).

15.3.1.1 Alumina Chemistry Under Acidic Conditions

The mechanism and products of acidic hydrolysis of Al^{3+} have been extensively studied using a wide variety of in situ and ex situ analytical techniques. These include potentiometric titrations (Brosset et al. 1954; Nail et al. 1976a), ^{27}Al NMR (Akitt et al. 1988; Akitt 1989; Casey 2006), SAXS (Rausch and Bale 1964; Bottero et al. 1982) and X-ray diffraction (Johansson 1960; Hsu and Bates 1964; Rowsell and Nazar 2000).

The process starts at pH < 3 with an unhydrolysed, mononuclear $[Al(H_2O)_6]^{3+}$ species, which with increasing pH hydrolyses according to the following idealised equations (Brinker and Scherer 1990):

$$[Al(H_2O)_6]^{3+} + xH_2O \rightarrow [Al(OH)_x(H_2O)_{6-x}]^{(3-x)+} + xH_3O^+$$

where x defines the extent of hydrolysis (i.e. the OH/Al ratio ranging from 0 to 3).

The further polycondensation of the so formed $[Al(OH)_x(H_2O)_{6-x}]^{(3-x)+}$ species and how these relate to the final solid Al-polymorphs have been extensively studied, yet the mechanisms are still controversial (Bi et al. 2004 and references therein). Essentially, two condensation mechanisms have been proposed: the "core-links" and the "cagelike" models (Bi et al. 2004).

According to the "core-links" model, the condensation of hexameric $[Al_6(OH)_{12}(H_2O)_{12}]^{6+}$ rings or $[Al_{10}(OH)_{22}(H_2O)_{16}]^{8+}$ double rings leads to larger sheetlike structures. In this case, $[Al_{54}(OH)_{144}]^{18+}$ was proposed to be the last species in the series, before the precipitation of a solid colloidal entity of the $[Al(OH)_3]_n$ type takes place (Bi et al. 2004). These colloids are expected to exhibit a local sheet-structure resembling that of the crystalline $Al(OH)_3$ phases. This model is primarily based on potentiometric titrations (Brosset et al. 1954; Stol et al. 1976) combined with X-ray diffraction analyses (Hsu and Bates 1964). Although the "core-links" model explains well the various titration characteristics, it lacks sufficient structural evidence for the proposed hexameric units and their consequent condensation products.

On the other hand, the "cagelike" model considers the well-characterised tridecamer $[(AlO_4)\,Al_{12}(OH)_{24}(H_2O)_{12}]^{7+}$ complex ion (Johansson 1960; Johansson et al. 1960) and other similar structures (Casey 2006) to be the actual primary building units in the alumina system. These primary structures are thought to be involved in the nucleation and growth of amorphous colloidal particles and their transformation to various crystalline polymorphs (Bottero et al. 1987; Fu et al. 1991). The tridecamer unit is also known as the Keggin Al_{13} structure, and it has been shown that such units exhibit a very high stability (up to several years) (Casey 2006). The presence of the Keggin ion in aluminate solutions can be easily identified through ^{27}Al NMR, and this method has thus been the primary tool to study the growth mechanisms and structures involving Keggin complex ions (Akitt 1989). Similarly, the structure of another large Al_{30} cation, $[Al_{30}O_8(OH)_{56}(H_2O)_{26}]^{18+}$, composed of two δ-Keggin units linked via four AlO_6 units (Fig. 15.5) has also been revealed by ^{27}Al NMR (Rowsell and Nazar 2000; Allouche et al. 2000; Casey 2006).

It is important to emphasise that depending on reaction conditions, the formation of other polynuclear species has been predicted. However, due to physical limitations of analytical tools (insufficient specificity allowing to distinguish various AlO_6-based species) such as the aforementioned ^{27}Al NMR, many of these species have so far not been characterised or even identified (Casey 2006). Hence, results from the experiments conducted under similar conditions are often interpreted by using either the "core-links" or the "cagelike" model (see the next paragraph). There have been attempts to consolidate the "core-links" and the "cagelike" models by reinterpreting the various experimental data and creating a "continuous" model (Bi et al. 2004). This unified model assumes that the polynuclear species transform

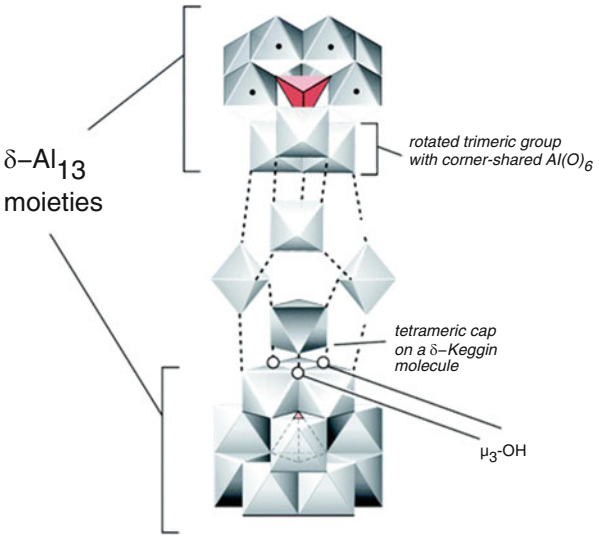

Fig. 15.5 $[Al_{30}O_8(OH)_{56}(H_2O)_{26}]^{18+}$ (aq) (Al_{30}) complex ion shown in a polyhedral exploded view. This structure can be viewed as two Keggin units (Al_{13}) joined by four AlO_6 octahedra. Al_{13} and Al_{30} species are 1 and 2 nm in size, respectively (Printed with permission from Casey (2006). Copyright American Chemical Society 2006)

dynamically through different intermediate stages, where the long-lived Keggin complex ions form upon ageing (i.e. the ion is stable as long as pH or temperature does not drastically change), but the validity of this combined model is still debated.

For instance, Nail et al. studied the early stages of amorphous alumina gel formation from $AlCl_3$ and $Al_2(SO_4)_3$ solutions and postulated a mechanism in which the evolution of polynuclear species to a solid colloidal precipitate was a stepwise process leading to the condensation of hexamers (Nail et al. 1976a). Depending on the original counter anion in the Al^{3+} solution, the colloidal precipitates were suggested to be composed of ~10 six-membered rings for Cl^- and only ~3 for SO_4^{2-}. Leetmaa et al. studied products forming under nearly identical conditions by means of ^{27}Al NMR and infrared/Raman spectroscopy (Leetmaa et al. 2014). Yet, their data also revealed that the products were primarily composed of polynuclear chains of highly distorted aluminium-based octahedra for the Cl^- system and of sulphate-stabilised Keggin Al_{13} clusters for the SO_4^{2-} system. Perry and Shafran evaluated the optimum conditions for the formation of polynuclear Al complexes and found that the neutralisation of $AlCl_3$ and $Al(NO_3)_3$ by KOH and $KHCO_3$ at low ionic strengths favours the formation of Al_{13} clusters and larger polymers (Perry & Shafran 2001). In contrary, in the presence of sulphates, the resulting products were primarily Al_{13} clusters, which was expected due to the stabilisation of the clusters by SO_4^{2-}.

The above-cited studies show that we have been learning more and more about the structures and the synthetic routes for the various polynuclear species for alumina under acidic conditions. Such insight is very important for the systematic analysis of the process, because the mechanistic details of the interplay of the various clusters on the path the crystalline phase remain rather vague at the moment.

15.3.1.2 Alumina Chemistry Under Alkaline Conditions

Processing of bauxite ores (aluminium-rich ores containing primarily gibbsite, boehmite and diaspore) under alkaline conditions is known as the Bayer method, and it is used to form also gibbsite and nordstrandite (Counter et al. 1997). The speciation of Al in basic solutions is rather complex and unsurprisingly a subject of controversy (Sipos 2009). Furthermore, little is known about any polynuclear complex ions that may form under these conditions. In fact, under highly alkaline conditions, the aluminate systems are considered to be actual solutions (see Fig. 15.1b), rather than colloidal systems, as was demonstrated, for instance, by light scattering or infrared and Raman spectroscopies (Li et al. 2003; Sipos 2009). Typically among the aqueous species, only tetrahedral $[Al(OH)_4]^-$ is expected to be present at pH > ~8–9 (Moolenaar et al. 1970; van Straten et al. 1984; Swaddle et al. 1994; Li et al. 2003; Sipos 2009). Some other mononuclear species such as linear $[AlO_2]^-$ and square planar $[Al(OH)_4(H_2O)_2]^-$ complexes may also be present (Gerson et al. 1996), but at insignificant concentrations (Swaddle et al. 1994; Sipos et al. 1998; Sipos 2009). At pH > 13, Al^{3+} can exist as either $[Al(OH)_5]^{2-}$ or $[Al(OH)_6]^{3-}$ (Akitt and Gessner 1984; Barcza and Pálfalvi-Rózsahegyi 1989; Buvári-Barcza et al. 1998), but again these two species are minority species (Sipos 2009) compared to the main $[Al(OH)_4]^-$ species. Using computational approaches, Gale et al. showed that at alkaline conditions dimeric complexes like $[(HO)_3Al(OH)_2Al(OH)_3]^{2-}$ should also be expected (Gale et al. 1998), while the presence (or significance) of higher polynuclear species is still a subject of controversy (an insightful discussion is given in Sipos (2009) and the references therein).

It is known that aluminium in amorphous precipitates is octahedrally coordinated in the same way as it is later in crystalline phases (Tettenhorst and Hofmann 1980; Wefers and Misra 1987). Upon precipitation from acidic solutions, independent of the actual condensation mechanism and possible speciation, one can assume that Al^{3+} also condenses into solids with a sixfold coordination. However, in the Bayer process, the dominant solution species, i.e. the $[Al(OH)_4]^-$ ion, exhibits a fourfold coordination. Hence, one might rationalise the nucleation stage in terms of a transition product, in which the realignment of ligands would occur to establish the octahedral geometry by a swap from the tetrahedral one. The question arises whether abundant $[Al(OH)_4]^-$ species constitute a monomer in crystal growth or whether there are actually other minority species which control the process. Gerson et al. carried out semiempirical quantum modelling of various mononuclear, dimeric, trimeric and tetrameric species in caustic aluminate solutions and suggested a mechanism and possible pathway in which a minority tetrahedral $[Al(OH)_3(H_2O)]$ complex could dimerise and then transform to the tetramer, via a transient trimer moiety (Gerson et al. 1996). In such a tetramer, a central octahedral Al^{3+} ion would be surrounded by three tetrahedral counterparts. However, results from conductivity studies combined with viscosity measurements of caustic aluminate solution were interpreted in terms of the formation of the

$[Al_6(OH)_{24}]^{6-}$ (Barcza and Pálfalvi-Rózsahegyi 1989; Buvári-Barcza et al. 1998) or $[Al_6(OH)_{22}]^{4-}$ moieties (Sipos et al. 1998). In such species, octahedral Al^{3+} geometry dominates, yet actual structural evidence for the proposed mechanisms is still lacking to say the least (Sipos 2009). In more dilute caustic solutions (i.e. [NaOH] / [Al] $\sim$ 1, and [NaOH] $\sim$ [Al] $\sim$ 1.0 mol/L), a polynuclear species in a size range comparable with that of Keggin Al_{13}-like species was proposed based on primarily light scattering evidence (Li et al. 2003, 2005a). Similar colloidal polynuclear aluminate structures were suggested based on optically clear supersaturated aluminate Bayer liquors analysed by cryo-vitrification of solutions at different stages and subsequent imaging by transmission electron microscopy (Counter et al. 1999). In these systems, the Keggin Al_{13}-like species were assumed to be primarily six-coordinated, and their existence in the Bayer process could provide a conceptual link between the mechanisms of $Al(OH)_3$ precipitation from the acidic and alkaline solutions. Finally, the critical nuclei size for gibbsite that forms as an end product in the Bayer process was calculated to have a radius of $\sim$ 1.2 nm (Rossiter et al. 1998), which is in line with the size range of Keggin ions and other small polynuclear oligomers (cf. Fig. 15.5). This might suggest that Keggin ions are sort of a universal "precursor" phase in alumina system regardless of conditions. This is an interesting hypothesis, but yet it has to be confirmed.

To illustrate the influence of physicochemical conditions and speciation onto the nucleation of phases precipitating from aluminate solutions, let us consider the investigations reported by Li et al. concerning the growth of gibbsite and bayerite through the Bayer process (Li et al. 2003, 2005a). The authors studied precipitation using dynamic light scattering to derive particle size distribution and X-ray diffraction for phase identification. Their data showed that dilute solutions ($\left[Al^{3+}\right] \leq 0.82$ M and [NaOH] $\leq$ 1.0 M) yielded bayerite and the concentrated ones ($\left[Al^{3+}\right] > 2.05$ M and [NaOH] $>$ 2.5 M) gibbsite, whereas a dimorphic product precipitated at intermediate concentrations ($0.82 < \left[Al^{3+}\right] \leq 2.05$ M and $1.0 <$ [NaOH] $\leq$ 2.5 M). To explain their results, the authors proposed a growth mechanism that took into account differences in speciation in the original aluminate solutions and was dependent on concentration. For dilute systems (Fig. 15.6a), they suggested that the process started with Keggin-like complex ions (1) that further aggregated and oligomerised to larger clusters (2); these coalesced to amorphous particles (3), which then lead to the rapid growth of nuclei (of pseudoboehmite) and/or pseudo-spinel phases (4), which transformed into pseudoboehmite (5) and then crystallised to a more stable bayerite phase. However, for concentrated solutions (Fig. 15.6b), the process originally involved small aluminate species such as ion pairs, dimers and trimers rather than the large Keggin ions (1), followed by formation of a loose Al^{3+}-containing oligomeric network (2), its initial densification to form a cluster (3), further densification to form a crystalline core (4), densification of the core and nuclei agglomeration (5) and final formation of a gibbsite crystal (6).

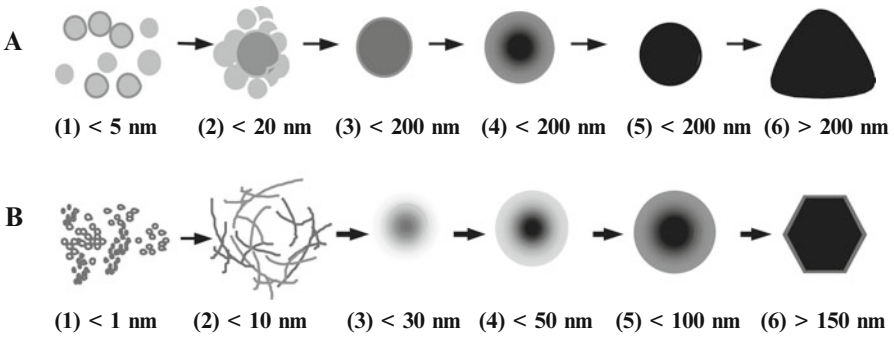

Fig. 15.6 A schematic representation of the formation of crystalline aluminium hydroxide from sodium aluminate solutions: (**a**) dilute solutions and (**b**) concentrated solutions. The size ranges indicated are speculative (Adapted and printed with permission from Li et al. (2005a). Copyright Elsevier 2005)

15.4 Outlook

This chapter highlights the extensive research carried out to unravel the mechanisms and pathways of silica and alumina colloid formation, with regard to both natural processes and industrial applications. Substantial advances in in situ scattering and imaging techniques have allowed to characterise the early stages of colloidal growth and aggregation; however, we are still facing substantial gaps in the molecular-level mechanistic understanding of the condensation reactions leading to the nucleation of the primary particles. This is particularly true for the alumina system where analytical limitations have so far hindered clear identification of all the polynuclear species forming in aluminate solutions, making it even harder to define their role in the formation of alumina colloids. For the silica system, the presence of polynuclear species seems of minor importance and colloid formation is more dependent on the behaviour of the monomeric silica. Whether silica nanoparticle growth occurs via the aggregation of primary particles or the addition of monomeric silica to existing particles is however still debated. It is evident that before we can formulate a fully coherent picture of silica and alumina colloid formation, more studies need to focus on the molecular characterisation of the condensation reactions and the nucleation of the primary particles. This is challenging with the current analytical limitations and the technical difficulties associated with these observations. However, in situ scattering and imaging techniques are constantly improving in resolution, with regard to both time and space. Also, the importance of silica and alumina nanophases for industrial processes further accelerates progress in this field, suggesting that a major breakthrough may come soon.

References

Ab Rahman I, Padavettan V (2012) Synthesis of silica nanoparticles by Sol-gel: size-dependent properties, surface modification, and applications in silica-polymer nanocomposites—a review. J Nanomater 2012:1687–4110

Akitt JW (1989) Multinuclear studies of aluminium compounds. Prog Nucl Magn Reson Spectrosc 21(1–2):1–149

Akitt JW, Gessner W (1984) Aluminium-27 nuclear magnetic resonance investigations of highly alkaline aluminate solutions. J Chem Soc Dalton Trans 1984:147–148

Akitt JW, Gessner W, Weinberger M (1988) High-field aluminium-27 nuclear magnetic resonance investigations of sodium aluminate solutions. Magn Reson Chem 25(12):1047–1050

Alexander GB (1954) The polymerisation of monosilicic acid. J Am Chem Soc 76(8):2094–2096

Allouche L, Gérardin C, Loiseau T, Férey G, Taulelle F (2000) Al30: a giant aluminum polycation. Angew Chem Int Ed 39(3):511–514

Bagwe RP, Hilliard LR, Tan WH (2006) Surface modification of silica nanoparticles to reduce aggregation and nonspecific binding. Langmuir 22:4357–4362

Bale HD, Schmidt PW (1959) Small angle X-ray scattering from aluminium hydroxide gels. II. J Chem Phys 31(6):1612–1618

Barcza L, Pálfalvi-Rózsahegyi M (1989) The aluminate lye as a system of equilibria. Mater Chem Phys 21(4):345–356

Barisik M, Atalay S, Beskok A, Qian S (2014) Size dependent surface charge properties of silica nanoparticles. J Phys Chem C 118(4):1836–1842

Belton DJ, Deschaume O, Perry CC (2012) An overview of the fundamentals of the chemistry of silica with relevance to biosilicification and technological advances. FEBS J 279(10):1710–20

Benning LG, Phoenix V, Mountain BW (2005) Biosilicification: the role of cyanobacteria in silica sinter deposition. In: Gadd GM, Semple KT, Lappin-Scott HM (eds) Micro-organisms and earth systems: advances in geomicrobiology, SGM Symposium. Cambridge University Press, Cambridge, pp 131–150

Besselink R, Stawski TM, Castricum HL, ten Elshof JE (2013) Evolution of microstructure in mixed niobia-hybrid silica thin films from sol-gel precursors. J Colloid Interface Sci 404:24–35

Bi S, Wang C, Cao Q, Zhang C (2004) Studies on the mechanism of hydrolysis and polymerization of aluminum salts in aqueous solution: Correlations between the “Core-links” model and “Cage-like” Keggin-Al 13 model. Coord Chem Rev 248:441–455

Bogush GH, Zukoski CF (1991) Uniform silica particle-precipitation – an aggregation growth model. J Colloid Interface Sci 142(1):19–34

Bottero JY, Tchoubar D, Cases JM, Fiessinger F (1982) Investigation of the hydrolysis of aqueous solutions of aluminum chloride. 2. Nature and structure by small-angle x-ray scattering. J Phys Chem 86(18):3667–3673

Bottero JY, Axelos M, Tchoubar D, Cases JM, Fripiat JJ, Fiessinger F (1987) Mechanism of formation of aluminium trihydroxide from Keggin Al13 polymers. J Colloid Interface Sci 117(1):47–57

Boukari H, Long GG, Harris MT (2000) Polydispersity during the formation and growth of the Stober silica particles from small-angle X-ray scattering measurements. J Colloid Interface Sci 229(1):129–139

Bradley SM, Hanna JV (1994) 27Al and 23Na MAS NMR and powder X-ray diffraction studies of sodium aluminate speciation and the mechanistics of aluminium hydroxide precipitation upon acid hydrolysis. J Am Chem Soc 116:7771–7783

Brinker CJ, Scherer GW (1990) Sol-gel science: the physics and chemistry of sol-gel processing. Academic, London

Brosset C, Biedermann G, Gunnar SL (1954) Studies on the hydrolysis of metal ions. XI. The aluminium ion, Al3+. Acta Chem Scand 8:1917–1926

Busing WR, Levy HA (1958) A single crystal neutron diffraction study of diaspore, AlO(OH). Acta Crystallogr 11:798–803

Buvári-Barcza Á, Rózsahegyi M, Barcza L (1998) Hydrogen bonded associates in the Bayer process (in concentrated aluminate lyes): the mechanism of gibbsite nucleation. J Mater Chem 8:451–455

Caho GY, Baker J, Sabina AP, Roberts AC (1985) Doyleite, a new polymorph of Al(OH)3, and its relationship to bayerite, gibbsite and nordstrandite. Can Mineral 23:21–28

Carcouet CCMC, van de Put MWP, Mezari B, Magusin PCMM, Laven J, Bomans PHH et al (2014) Nucleation and growth of monodisperse silica nanoparticles. Nano Lett 14(3):1433–1438

Carroll S, Mroczek E, Alai M, Ebert M (1998) Amorphous silica precipitation (60 to 120 degrees C): comparison of laboratory and field rates. Geochim Cosmochim Acta 62(8):1379–1396

Casey WH (2006) Large aqueous aluminium hydroxide molecules. Chem Rev 106(1):1–16

Cesteros Y, Salagre P, Medina F, Sueiras JE (1999) Several factors affecting faster rates of gibbsite formation. Chem Mater 11:123–129

Christoph GG, Corbató CE, Hofman DA, Tettenhorst R (1979) The crystal structure of boehmite. Clay Clay Miner 27:81–86

Conrad CF, Icopini GA, Yasuhara H, Bandstra JZ, Brantley SL, Heaney PJ (2007) Modeling the kinetics of silica nanocolloid formation and precipitation in geologically relevant aqueous solutions. Geochim Cosmochim Acta 71(3):531–542

Counter J, Gerson A, Ralston J (1997) Caustic aluminate liquors: preparation and characterisation using static light scattering and in situ X-ray diffraction. Colloids Surf A Physicochem Eng Asp 126(2–3):103–112

Counter JA, Addai-Mensah J, Raiston J (1999) The formation of Al(OH)3 crystals from supersaturated sodium aluminate solutions revealed by cryovitrification-transmission electron microscopy. Colloids Surf A Physicochem Eng Asp 154(3):389–398

De Yoreo JJ, Sommerdijk NAJM, Dove PM (2017) Nucleation pathways in electrolyte solutions. In: Van Driessche AES, Kellermeier M, Benning LG, Gebauer D (eds) New perspectives on mineral nucleation and growth, Springer, Cham, pp 1–24

Demichelis R, Catti M, Dovesi R (2009) Structure and stability of the Al(OH)3 polymorphs doyleite and nordstrandite: a quantum mechanical ab initio study with the CRYSTAL06 code. J Phys Chem C 113:6785–6791

Dietzel M (2000) Dissolution of silicates and the stability of polysilicic acid. Geochim Cosmochim Acta 64(19):3275–3281

Fouilloux S, Tache O, Spalla O, Thill A (2011) Nucleation of silica nanoparticles measured in situ during controlled supersaturation increase: restructuring toward a monodisperse nonspherical shape. Langmuir 27(20):12304–12311

Fu G, Nazar LF, Bain AD (1991) Ageing processes of alumina sol-gels: characterization of new aluminium polyoxycations by 27Al NMR spectroscopy. Chem Mater 3:602–610

Gale JD, Rohl AL, Watling HR, Parkinson GM (1998) Theoretical investigation of the nature of aluminum-containing species present in alkaline solution. J Phys Chem B 102(50):10372–10382

Gerson AR, Raiston J, Smart RSC (1996) An investigation of the mechanism of gibbsite nucleation using molecular modelling. Colloids Surf A Physicochem Eng Asp 110(1):105–117

Gong X, Nie Z, Qian M, Liu J, Pederson LA, Hobbs DT, McDuffle NG (2003) Gibbsite to boehmite transformation in strongly caustic and nitrate environments. Ind Eng Chem Res 42:2163–2170

Green DL, Lin JS, Lam YF, Hu MZC, Schaefer DW, Harris MT (2003) Size, volume fraction, and nucleation of Stober silica nanoparticles. J Colloid Interface Sci 266(2):346–358

Gunnarsson I, Arnorsson S (2000) Amorphous silica solubility and the thermodynamic properties of H4SiO4 degrees in the range of 0 degrees to 350 degrees C at P-sat. Geochim Cosmochim Acta 64(13):2295–2307

Gunnarsson I, Arnorsson S (2005) Impact of silica scaling on the efficiency of heat extraction from high-temperature geothermal fluids. Geothermics 34(3):320–329

Heaney PJ, Prewitt CT, Gibbs GV (1994) Silica: Physical behaviour, geochemistry & materials applications. Reviews in mineralogy Vol 29, Princeton, pp. 606

Hench LL, West JK (1990) The sol-gel process. Chem Rev 90:33–72

Herdianita NR, Browne PRL, Rodgers KA, Campbell KA (2000) Mineralogical and textural changes accompanying ageing of silica sinter. Miner Deposita 35(1):48–62

Hsu PH, Bates TF (1964) Formation of X-ray amorphous and crystalline aluminium hydroxides. Mineral Mag 33:749–768

Hsu H-W, Postberg F, Sekine Y, Shibuya T, Kempf S, Horányi M, Juhász A, Altobelli N, Suzuki K, Masaki Y, Kuwatani T, Tachibana S, Sirono S, Moragas-Klostermeyer G, Srama R (2015) Ongoing hydrothermal activities within Enceladus. Nature 519:207–210

Hu C, Liu H, Qu J, Wang D, Ru J (2006) Coagulation behavior of aluminium salts in eutrophic water: significance of Al13 species and pH control. Environ Sci Technol 40(1):325–331

Icopini GA, Brantley SL, Heaney PJ (2005) Kinetics of silica oligomerization and nanocolloid formation as a function of pH and ionic strength at 25 C. Geochim Cosmochim Acta 69:293–303

Iler RK (1979) The colloid chemistry of silica and silicates. Cornell University Press, Ithaca

Johansson G (1960) On the crystal structure of some basic aluminium salts. Acta Chem Scand 14:771–773

Johansson G, Lundgren G, Sillen LG, Soderquist R (1960) The crystal structure of a basic aluminum sulfate and the corresponding selenite. Acta Chem Scand 14:769–771

Kasprzyk-Hordern B (2004) Chemistry of alumina, reactions in aqueous solution and its application in water treatment. Adv Colloid Interface Sci 110:19–48

Keller WD (1978) Diaspore recrystallized at low temperature. Am Mineral 63:326–329

Kley M, Kempter A, Boyko V, Huber K (2014) Mechanistic studies of silica polymerization from supersaturated aqueous solutions by means of time-resolved light scattering. Langmuir 30(42):12664–12674

Kloprogge JT, Duong LV, Wood BJ, Frost RL (2006) XPS study of the major minerals in bauxite: gibbsite, bayerite and (pseudo-) boehmite. J Colloid Interface Sci 296:572–576

Kobayashi M, Juillerat F, Galletto P, Bowen P, Borkovec M (2005) Aggregation and charging of colloidal silica particles: effect of particle size. Langmuir 21(13):5761–5769

Leetmaa K, Gomez MA, Becze L, Guo F, Demopoulos GP (2014) Comparative molecular characterization of aluminum hydroxy-gels derived from chloride and sulphate salts. J Chem Technol Biotechnol 89(2):206–213

Levin I, Brandon D (1998) Metastable alumina polymorphs: crystal structure and transition sequences. J Am Ceram Soc 81(8):1995–2012

Li H, Addai-Mensah J, Thomas JC, Gerson AR (2003) A study of colloidal Al(III)-containing species in fresh/caustic aluminate solutions. Colloids Surf A Physicochem Eng Asp 223:83–94

Li H, Addai-Mensah J, Thomas JC, Gerson AR (2005a) The crystallization mechanism of Al(OH)3 from sodium aluminate solutions. J Cryst Growth 279:508–520

Li H, Addai-Mensah J, Thomas JC, Gerson AR (2005b) The influence of Al(III) supersaturation and NaOH concentration on the rate of crystallization of Al(OH)3 precursor particles from sodium aluminate solutions. J Colloid Interface Sci 286:511–519

Li Y, Zhang Y, Chen F, Yang C, Zhang Y (2011) Polymorphic transformation of aluminum hydroxide precipitated from reactive NaAl(OH)4-NaHCO3 solution. Cryst Growth Des 11:1208–1214

Loh JSC, Fogg AM, Watling HR, Parkinson GM, O'Hare D (2000) A kinetic investigation of gibbsite precipitation using in situ time resolved energy dispersive X-ray diffraction. Phys Chem Chem Phys 2:3597–3604

Marshall WL, Chen CTA (1982) Amorphous silica solubilities. 5. Predictions of solubility behaviour in aqueous electrolyte solutions of 300°C. Geochim Cosmochim Acta 46(2):289–291

Matsoukas T, Gulari E (1989) Monomer-addition growth with a slow initiation step: a growth model for silica particles from alkoxides. J Colloid Interface Sci 132(1):13–21

Meier D, Gunnlaugsson E, Gunnarsson I, Jamtveit B, Peacock CL, Benning LG (2014) Microstructural and chemical variations in silica-rich precipitates at the Hellisheidi geothermal power plant. Min Mag 78(6):1381–1389

Momma K, Izumi F (2011) VESTA 3 for three-dimensional visualization of crystal, volumetric and morphology data. J Appl Crystallogr 44:1272–1276

Moolenaar RJ, Evans JC, McKeever LD (1970) Structure of the aluminate ion in solutions at high pH. J Phys Chem 74(20):3629–3636
Mountain BW, Benning LG, Boerema JA (2003) Experimental studies on New Zealand hot spring sinters: rates of growth and textural development. Can J Earth Sci 40(11):1643–1667
Nail SL, White JL, Hem SL (1976a) Structure of aluminium hydroxide gel I: initial precipitate. J Pharm Sci 65(8):1189–1191
Nail SL, White JL, Hem SL (1976b) Structure of aluminium hydroxide gel II: aging mechanism. J Pharm Sci 65(8):1192–1195
Nail SL, White JL, Hem SL (1976c) Structure of aluminium hydroxide gel III: mechanism of stabilization by sorbitol. J Pharm Sci 65(8):1195–1198
Noguera C, Fritz B, Clement A (2015) Precipitation mechanism of amorphous silica nanoparticles: a simulation approach. J Colloid Interface Sci 448:553–563
Pancost RD, Pressley S, Coleman JM, Benning LG, Mountain BW (2005) Lipid biomolecules in silica sinters: indicators of microbial biodiversity. Environ Microbiol 7(1):66–77
Panias D, Asimidis P, Paspaliaris I (2001) Solubility of boehmite in concentrated sodium hydroxide solutions: model development and assessment. Hydrometallurgy 59:15–29
Patwardhan SV (2011) Biomimetic and bioinspired silica: recent developments and applications. Chem Commun 47(27):7567–7582
Perry CC, Keeling-Tucker T (2000) Biosilicification: the role of the organic matrix in structure control. J Biol Inorg Chem 5(5):537–550
Perry CC, Shafran KL (2001) The systematic study of aluminium speciation in medium concentrated aqueous solutions. J Inorg Biochem 87:115–124
Petz JJI (1968) Structure of aluminium hydroxide gel. J Chem Phys 48(2):909–911
Rausch WV, Bale HD (1964) Small-angle X-ray scattering from hydrolyzed aluminium nitrate solutions. J Chem Phys 40:3391–3394
Rossiter DS, Fawell PD, Ilievski D, Parkinson GM (1998) Investigation of the unseeded nucleation of gibbsite, Al(OH)3, from synthetic bayer liquors. J Cryst Growth 191:525–536
Rothbauer R, Zigan F, O'Daniel H (1967) Verfeinerung der struktur des bayerits, Al(OH)3. Z Kristallogr Krist 125:317–331
Rothbaum HP, Rohde AG (1979) Kinetics of silica polymerization and deposition from dilute-solutions between 5°C and 180°C. J Colloid Interface Sci 71(3):533–559
Rousseaux JM, Weisbecker P, Muhr H, Plasari E (2002) Aging of precipitated amorphous alumina gels. Ind Eng Chem Res 41(24):6059–6069
Rowsell J, Nazar LF (2000) Speciation and thermal transformation in alumina sols: structures of the polyhydroxyoxoaluminum cluster [Al30O8(OH)56(H2O)26]18+ and its δ-Keggin moieté. J Am Chem Soc 122(15):3777–3778
Ruan HD, Frost RL, Kloprogge JT (2001) Comparison of Raman spectra in characterizing gibbsite, bayerite, diaspore and boehmite. J Raman Spectrosc 32:745–750
Ryan JN, Elimelech M (1996) Colloid mobilization and transport in groundwater. Colloids Surf A Physicochem Eng Asp 107:1–56
Saalfeld H, Jarchow O (1968) Die Kristallstruktur von Nordstrandit, Al(OH)3. Neues Jahrb Mineral Abh 109:185–191
Saalfeld H, Wedde M (1974) Refinement of the crystal structure of gibbsite, Al(OH)3. Z Kristallogr Krist 139:129–135
Sipos P (2009) The structure of Al(III) in strongly alkaline solutions – a review. J Mol Liq 146:1–14
Sipos P, Capewell SG, May PM, Hetter G, Laurenczy G, Lukács F, Roulet R (1998) Spectroscopic studies of the chemical speciation in concentrated alkaline solutions. J Chem Soc Dalton Trans 1998:3007–3012
Smith SJ, Amin S, Woodfield BF, Boerio-Goates J, Campbell BJ (2013) Phase progression of γ-Al2O3 nanoparticles synthesized in a solvent deficient environment. Inorg Chem 52:4411–4423
Squyres SW, Arvidson RE, Ruff S, Gellert R, Morris RV, Ming DW et al (2008) Detection of silica-rich deposits on Mars. Science 320(5879):1063–1067

Stawski TM, Benning LG (2013) Chapter 5: SAXS in inorganic and bioinspired research. Methods Enzymol 532:95–127

Stöber W, Fink A, Bohn E (1968) Controlled growth of monodisperse silica spheres in micron size range. J Colloid Interface Sci 26(1):62–69

Stol RJ, van Helden AK, de Bruyn PL (1976) Hydrolysis-precipitation studies of aluminum (III) solutions. 2. A kinetic study and model. J Colloid Interface Sci 57(1):115–131

Swaddle TW, Salerno J, Tregloan PA (1994) Aqueous aluminates, silicates, and aluminosilicates. Chem Soc Rev 23:319–325

Tettenhorst R, Hofmann DA (1980) Crystal chemistry of boehmite. Clay Clay Miner 28(5):373–380

Tobler DJ, Benning LG (2013) In situ and time resolved nucleation and growth of silica nanoparticles forming under simulated geothermal conditions. Geochim Cosmochim Acta 114:156–168

Tobler DJ, Stefansson A, Benning LG (2008) In-situ grown silica sinters in Icelandic geothermal areas. Geobiology 6(5):481–502

Tobler DJ, Shaw S, Benning LG (2009) Quantification of initial steps of nucleation and growth of silica nanoparticles: an in-situ SAXS and DLS study. Geochim Cosmochim Acta 73(18):5377–5393

van Straten HA, Holtkamp BTW, de Bruyn PL (1984) Precipitation from supersaturated aluminate solutions: I. Nucleation and growth of solid phases at room temperature. J Colloid Interface Sci 98(2):342–362

Wang L, Zhao W, Tan W (2008) Bioconjugated silica nanoparticles: development and applications. Nano Res 1:99–115

Wefers K, Misra C (1987) Oxides and hydroxides of aluminium, Alcoa Technical Paper 19. Aluminium Company of America, Pittsburgh

Westall F, Walsh MM (2000) The diversity of fossil microorganisms in Archaen-age rocks. In: Seckbach J (ed) Journey to diverse microbial worlds. Kluwer, Amsterdam

Williams LA, Crerar DA (1985) Silica diagenesis 2: general mechanisms. J Sediment Petrol 55(3):312–321

Yokoi T, Sakamoto Y, Terasaki O, Kubota Y, Okubo T, Tatsumi T (2006) Periodic arrangement of silica nanospheres assisted by amino acids. J Am Chem Soc 128(42):13664–13665